Phys. Status Solidi A **209**, No. 5, 813–818 (2012) / **DOI** 10.1002/pssa.201100785

physica status solidi a
www.pss-a.com
applications and materials science

# Ultra-thin anodic alumina capacitor films for plastic electronics

**Andrei Ionut Mardare[1], Martin Kaltenbrunner[2], Niyazi Serdar Sariciftci[3], Siegfried Bauer[2], and Achim Walter Hassel[*,1]**

[1] Institute for Chemical Technology of Inorganic Materials, Johannes Kepler University, 4040 Linz, Austria
[2] Soft Matter Physics, Johannes Kepler University, 4040 Linz, Austria
[3] Institute for Physical Chemistry, Johannes Kepler University, 4040 Linz, Austria

Received 8 November 2011, revised 11 January 2012, accepted 7 February 2012
Published online 12 April 2012

**Keywords** anodic oxide film, plastic electronics, scanning droplet cell

[*] Corresponding author: e-mail achimwalter.hassel@jku.at, Phone: +43-732-24688702, Fax: +43-732-24688704

Ultrapure aluminium was thermally evaporated onto various plastics (polyethylene 2.6-naphthalate, PEN; polyethylene terephthalate, PET; polyimide, PI and glass for comparison) and potentiostatically anodized in a citric buffer. The anodisation procedure was monitored coulometrically and each alumina film formed was characterized by impedance spectroscopy. The resulting anodic alumina films were amorphous (proven by X-ray diffraction, XRD) and acted as dielectric material in a solid state capacitor with Au top electrode. The capacitors characteristics were evaluated using IV curves and frequency domain measurements. The performance of the capacitors demonstrated low leakage currents and low dielectric losses. The contrary properties capacity and breakdown voltage could be chosen by selecting the anodisation voltage. For each substrate apparent oxide formation factors and capacities were determined coulometrically. The ratio between apparent formation factor and projected area allowed determining the surface roughness. This surface roughness together with the high purity aluminium films and the anodisation compression was responsible for the unexpected high mechanical stability of this composite material.

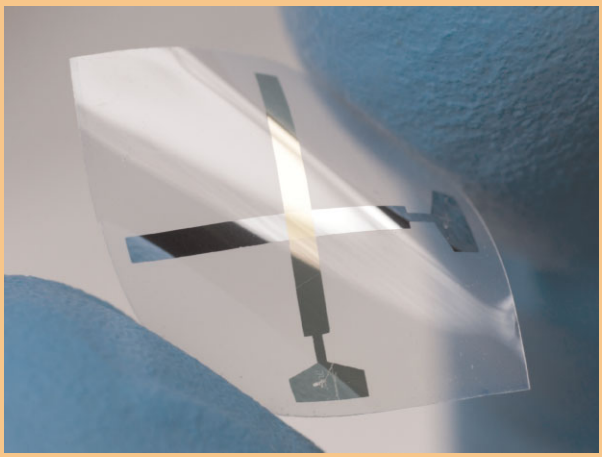



**1 Introduction** In plastic electronics polymer substrates are combined with stacks of thin metal, dielectric and semiconductor films to form flexible displays [1], solar cells [2], human machine interfaces [3], and sensors for biomedical sensing [4]. Basic circuit elements comprise transistors [5] and photo-diodes [6], but also passive elements such as conductors [7], resistors and capacitors [8]. While there has been tremendous success in the demonstration of active electronic components [9], there is a lack in developing passive elements, such as capacitors with very well controllable capacities.

In common electronics, capacitors often consist of aluminium or tantalum foils or sintered powders with their oxides as dielectric material. This is in particular true when a stable oxide film is required with low leakage current [10], low dielectric losses [11], low thermal coefficient [10] and high breakdown voltage [12, 13]. These oxides are formed anodically to achieve highest performance. Anodic oxide formation on these metals is a self-inhibiting process, thus it is self-healing and converging to a uniform film thickness for a given potential [14, 15]. The oxides on these metals grow according to the high field model [16]. Thus a further

improvement of the properties is not only possible by flash annealing [17] an interesting technique (not applicable in plastic electronics) but also by subsequent short pulse annealing [18].

The actual properties of the dielectric material can be easily tuned by the electrochemical process of anodisation. The high field oxide growth guarantees a film growth factor of 1.6 nm $V^{-1}$ [19] reducing the choice of the oxide film thickness to a simple control of the formation voltage or voltage scan rate. Here the method of choice is a potentiostatic anodization of aluminium to prepare well-defined aluminium oxide layers for capacitors on flexible substrates. It is also demonstrated that these oxides show a remarkable high mechanical stability as compared to text book values of the stress/strain stability of the ceramic aluminium oxide, resulting from the synergistic interaction of the anodisation process, the metal formation process and the structure of the plastics substrate.

**2 Experimental** Aluminium thin films were deposited at room temperature on various substrates from 99.9995% purity Al wires (Alfa Aesar) using the thermal evaporation technique. The target material was cut in short pieces and placed inside a tungsten coil. A high current passing through the coil ensured evaporation of Al through Joule heating. 150 nm thick Al films were deposited using a deposition rate of 2.5 nm $s^{-1}$. The substrate size was 15 mm × 15 mm and the substrate materials used were amorphous silica (microscope cover glasses) serving as reference films and three different plastics (50 μm thick): polyethylene 2.6-naphthalate (PEN), polyethylene terephthalate (PET) and polyimide (PI). The vacuum system (cylinder with a diameter of 300 mm) had a base pressure of $1 \times 10^{-3}$ Pa and the deposition distance was 120 mm. The Al film nanostructures on different substrates were analyzed by scanning electron microscopy (SEM) and atomic force microscopy (AFM) and the crystallographic properties were investigated by X-ray diffraction (XRD). For the AFM and XRD measurements, all plastic samples (foils) were glued onto glass substrates for ensuring flat surfaces.

For each sample, the Al thin film was locally anodized in citric acid/citrate buffer (0.265 g citric acid, 2.57 g sodium citrate in 100 ml DI water producing a pH 6.0) using a scanning droplet cell (SDC) [20]. After thermal pulling of a 2 mm diameter glass capillary, the diameter of the SDC tip was defined at 1.6 mm through mechanical polishing. The contact mode of the SDC was used for each anodization to take advantage of the higher reproducibility of the wetted area as compared to the free droplet mode [21]. This allows a direct comparison between Al films deposited on various substrates. For avoiding the electrolyte–air contact during anodization, a silicone gasket was formed at the tip of the SDC by dipping the glass capillary into liquid silicone followed by drying it in a nitrogen gas flow. The reference electrode (RE) used inside the SDC was a self-made agar-based μ-Ag/AgCl capillary RE [22] with a tip diameter of 100 μm. A gold band (99.999% Wieland Dentaltechnik, Germany) wrapped around the RE served as counter electrode (CE). The glass capillary containing the RE provided electrical insulation towards the CE. A potentiostat (Solartron SI 1287) in combination with a frequency response analyzer (Solartron SI 1260) was used for all electrochemical investigations, including impedance spectroscopy.

Solid state thin film capacitors were formed having the locally anodized Al as dielectric and a thermally evaporated Au layer as top electrode. *I–V* characteristics of the alumina capacitors were recorded with a Keithley 6430 source meter, dielectric spectra were taken with a Novocontrol Alpha-A high performance frequency analyzer over the frequency range from $10^4$ to $10^{-4}$ Hz.

**3 Results and discussion** After Al thin film depositions, the nanoscale features of the metallic layers were analyzed on different substrates. In Fig. 1 the SEM (top) and AFM (bottom) images of the Al surface is presented for samples deposited in the same evaporation batch. A typical fine grain structure can be observed on Al/glass samples with grains of approximately 20 nm. This structure changes when plastic substrates are used and bigger grains of around 100 nm can be observed for Al/PI. All samples were free of visible defects (e.g. pores, cracks, crevasses, etc.). The Al films deposited on plastics remained as stable and as compact as the one deposited on glass. This indicates a good adhesion during the evaporation on plastics and surface energies for incoming Al comparable with the deposition on glass, which allows a good surface diffusion during the film growth process. For each SEM image, a corresponding AFM scan is shown for each sample. The Al films on glass are smooth with RMS roughness of 1.7 nm. As soon as the substrate is replaced by plastics, the nanostructure changes, and the roughness values measured were 3.11, 4.29 and 4.79 nm for PEN, PET and PI, respectively. The films deposited on PEN substrates showed a more pronounced texture when compared with the glass substrates. Wrinkles which can spread across several μm and can be around 20 nm deep are observed. In the case of PET, the wrinkles become much sharper and in the case of PI the wavy

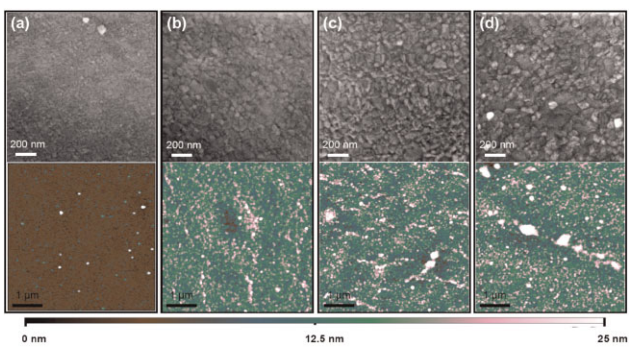


**Figure 1** (online colour at: www.pss-a.com) SEM (top) and AFM (bottom) imaging of Al thin films deposited on glass (a), PEN (b), PET (c) and PI (d).

aspect of the surface is replaced by a clustering of the grains producing high features with widths in the micrometer range. However, this micrometer-range feature of the plastics represents an almost macroscopic surface phenomenon which in principle should not hinder the anodic oxide growth process.

The crystallographic properties of the Al thin films deposited on different substrates were analyzed by XRD. In Fig. 2 the Al XRD spectra are shown for all samples. When deposited on glass, the main Al (111) peak is present at 38.47° and no other Al peak could be detected. A background, specific to the amorphous silica substrate, can be observed at low angles. For both polyethylene substrates (PEN, PET) the polymeric peaks are similar and still only one metal peak (Al (111)) can be observed. There should be no ambiguities assigning the XRD peaks, since at the positions of the next two intense Al peaks (Al (200) at 44.72° and Al (220) at 65.1°) no peak could be detected whatsoever [23]. In the last case of using PI as substrate for Al thin films, the polymer contribution to the diffraction pattern is reduced indicating a higher degree of amorphisation. Nevertheless, the Al (111) peak is still present at the same location as for the previous samples. Small deviations from the position of the Al peak measured on glass can be identified, but since these deviations are not bigger than 0.1° they can be attributed to small deviations from the horizontal plane due to sample preparation for XRD investigations. This can be better observed in the inset of Fig. 2 where a zoomed region of the scan is shown. The comparative XRD analysis shown in Fig. 2 clearly indicates that the Al films are growing on plastic substrates with a preferential (111) orientation, identical to the case of using glass substrates, with no indication of extra substrate/film crystallographic mismatch or adhesion problems.

Anodic oxide was grown potentiodynamically at a rate of 100 mV $s^{-1}$ on each Al thin film using the SDC. The maximum potential achieved during cyclic voltammetry was increased in 1 V steps until a final anodization potential of 10 V was reached. This step-wise growth of the anodic films allowed intermitting electrochemical impedance spectroscopy, i.e. a spectra after each successive step of oxide thickness increase [24]. In Fig. 3 the voltammogram series for Al anodizations on all four different substrates are presented. Due to the valve metal behaviour of Al, the high field model is appropriate to describe the oxide growth kinetics [16]. The oxidation current density shows a constant plateau in a potentiodynamic anodization (when the anodization rate is kept constant) due to Faraday's law expressing the proportionality between the charge consumed in the anodization process and the mass of the forming oxide [23]. The oxidation current plateau for anodization of the reference Al thin film sample deposited on glass has lead to the calculation of an oxide formation factor of 1.58 nm $V^{-1}$ which is consistent with data reported in the literature [16]. When using plastic as substrate, the Al oxidation current plateau showed an increased value for each polymer. This can in principle be attributed to a higher effective surface of the Al films when deposited on the plastic substrates. This idea is consistent with the SEM images presented in Fig. 1, where bigger grain sizes for Al can be observed for PEN, PET and PI substrates.

The charge consumed during the anodic oxide growth can be directly calculated by integrating the current curves. In Fig. 4 the current variation with time is presented for the potentiodynamic anodizations shown in Fig. 3. The different current plateaus for these substrates are also seen here. Integrating each cyclic voltammogram from the four shown series and summing the obtained values for the charge consumed in all previous oxidation steps has resulted in the determination of the charge needed for oxidation at a certain maximum applied potential. In the inset of Fig. 4 the charge density is plotted *versus* the anodization potential. A very

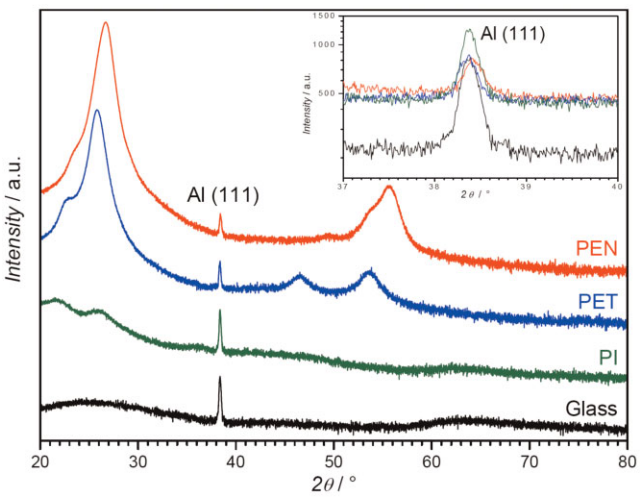


**Figure 2** (online colour at: www.pss-a.com) XRD spectra of Al thin films deposited on various substrates and enlarged Al(111) peak (inset).

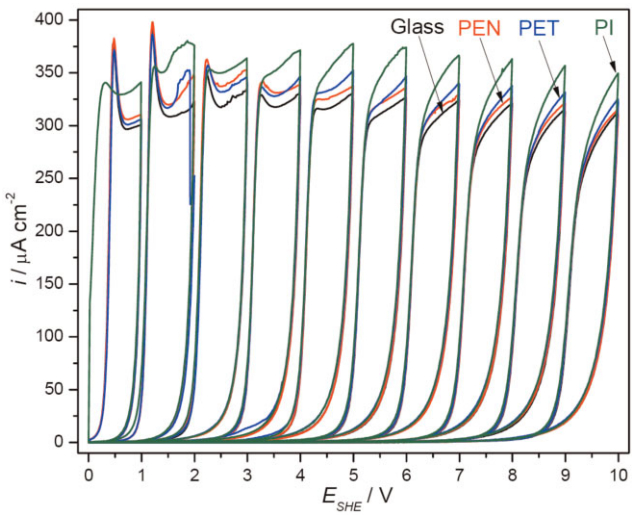


**Figure 3** (online colour at: www.pss-a.com) Voltammogram series for Al potentiodynamic anodizations (0.1 V $s^{-1}$) on different substrates.

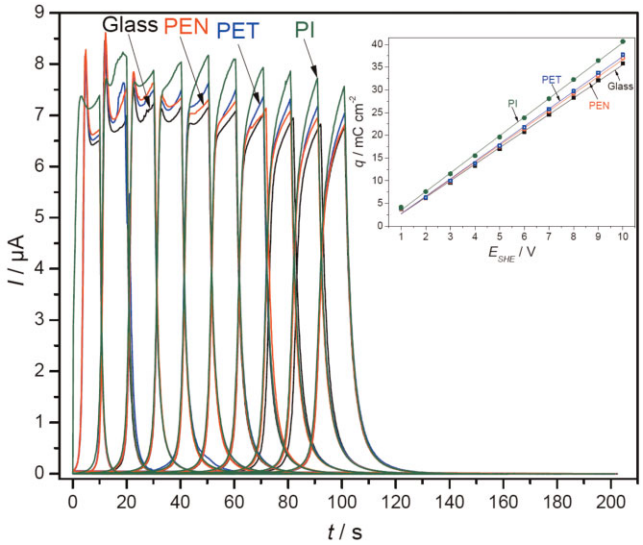


**Figure 4** (online colour at: www.pss-a.com) Time variation of anodization current and charge density (inset) for Al anodic oxide growth on various substrates.

good linear dependence can be observed for all samples between the charge needed for anodization and the applied potential, indicating a constant anodic charge factor. This suggests that independent on the substrate used, the Al thin films can be oxidized electrochemically without side reactions and as a result a dense ultra-thin oxide layer can be easily obtained [20].

Full spectra electrochemical impedance spectroscopy measurements were used for determining the electrical behaviour of the growing anodic oxide. After each anodization step (1 V) the impedance was measured for a frequency range between $10^5$ and 1 Hz. In Fig. 5 a typical series of impedance spectra (similar for all substrates used) is presented as measured on the Al/glass samples.

Increasing the anodization potential, both the impedance modulus and the phase dependencies on the frequency start to be shifted due to an increase in the oxide resistance and a decrease in its capacitance. This trend shows the thickness layer increase of the anodic oxide. For all samples and all used substrates, a simple RC-R equivalent circuit (representing the parallel oxide resistance and capacitance in series with the electrolyte resistance) was used for fitting the spectra. Again side reactions were excluded by the single time constant observable in the impedance spectra of Fig. 5.

From the measured oxide capacitances after fitting the impedance spectra, inverse capacitance could be plotted as a function of anodization potential. This dependence is seen in Fig. 6 for Al films deposited on all four substrates. A linear dependence between the inverse capacitance and the anodization potential is to be expected, since the oxide thickness depends linearly on the potential through the anodic oxide formation factor mentioned previously. The slopes of these curves will directly allow measuring the dielectric constant of the oxide.

Until this point, some information could be gathered from the anodization and impedance measurements. In Table 1 these results are summarized. The apparent oxide formation factors ($k'$) measured from the oxidation current plateaus of the cyclic voltammograms (Fig. 3), the apparent anodic charge factor ($q'$) measured from the slopes of the charge densities in Fig. 4 and the apparent dielectric constants measured from the slopes of the inverse capacitance curves (Fig. 6) are shown for all plastic substrates used and compared with the reference values measured on Al/glass. The oxide formation factor of alumina on plastics showed slightly increased values as compared with Al deposited on glass, reaching 1.74 nm V$^{-1}$ in the case of PI.

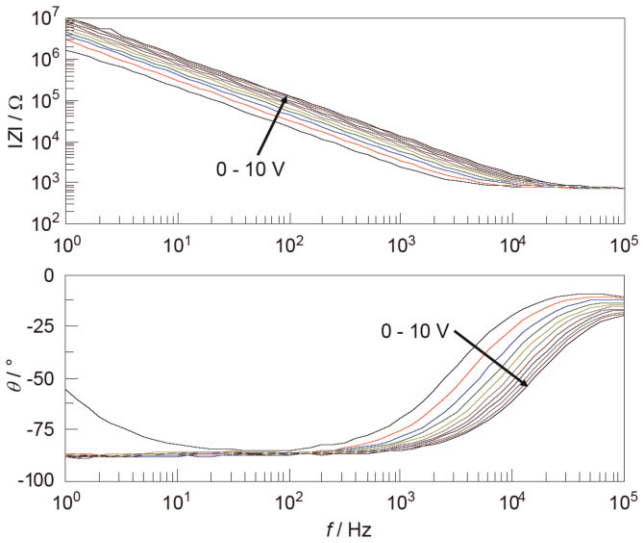


**Figure 5** (online colour at: www.pss-a.com) Typical oxide impedance (top) and phase shift (bottom) spectra measured *in situ* during the stepwise anodization of Al.

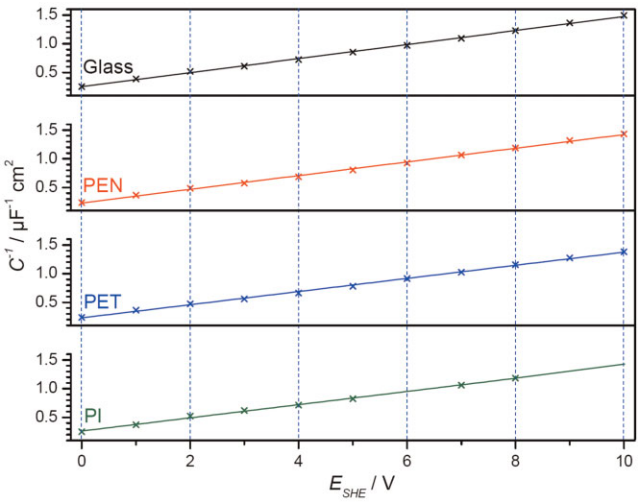


**Figure 6** (online colour at: www.pss-a.com) Oxide inverse capacitance dependence on the anodization potential for Al films deposited on various substrates.

**Table 1** Apparent oxide formation factors, anodic charge factors and permittivity for anodic oxidation of Al on various substrates.

| substrate | $k'$ (nm V$^{-1}$) | $q'$ (mC cm$^{-2}$ V$^{-1}$) | $\varepsilon'$ |
|---|---|---|---|
| glass | 1.58 | 3.64 | 14.6 |
| PEN | 1.63 | 3.76 | 15.5 |
| PET | 1.67 | 3.84 | 16.5 |
| PI | 1.74 | 4.09 | 17.1 |

**Table 2** Relative variation of the oxide formation factors, anodic charge factors and dielectric constants of alumina for plastic substrates as referenced to the glass substrates.

| substrate | $\Delta k$ (%) | $\Delta q$ (%) | $\Delta\varepsilon$ (%) |
|---|---|---|---|
| PEN | 3.2 | 3.3 | 6.2 |
| PET | 5.7 | 5.5 | 13 |
| PI | 10.1 | 12.4 | 17.1 |

This can be attributed to higher effective areas of the Al exposed to the electrolyte due to bigger grain sizes leading to rougher films. Accordingly, the anodic charge factor will be increased for plastic substrates due to the proportionality between the two parameters. Variation of the effective wetted area has also lead to an increase of the measured dielectric constant of anodic alumina formed on plastic substrates as compared with the case of glass substrates. Table 2 presents the percentage variation of the parameters measured during the anodic oxide growth of Al deposited on plastics as compared with the films deposited on glass. All effective factors measured increase with at least 3% when plastics are used as substrates, the higher variation being observed for PI. This can be correlated with higher surface roughness of the plastics as previously shown in Fig. 1.

Finally, the dielectric characterization of a thin film solid state capacitor comprising of a 9 nm thick oxide layer

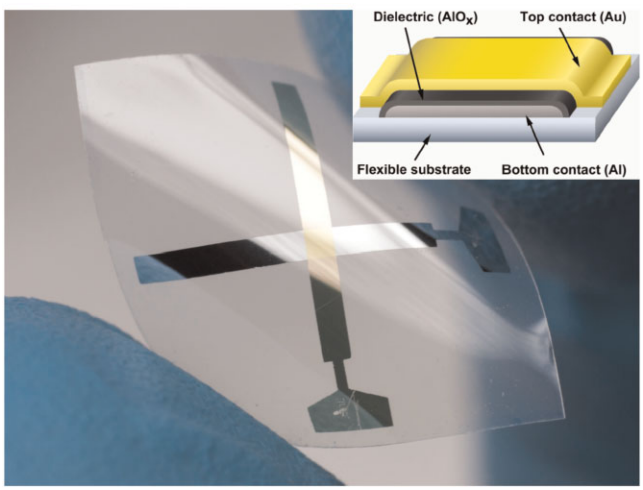


**Figure 7** (online colour at: www.pss-a.com) Photograph of a thin film capacitor on PEN, demonstrating the flexibility of the fabricated devices.

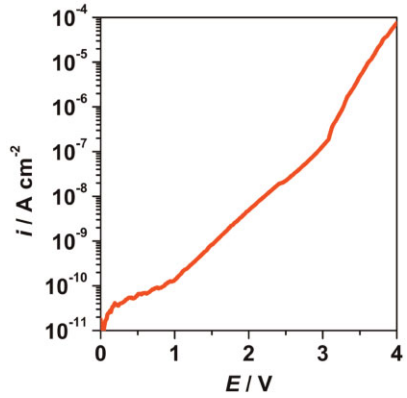


**Figure 8** (online colour at: www.pss-a.com) Au/$Al_2O_3$/Al/PEN capacitor leakage currents.

(formed with 4 V anodization potential on the 2.6 nm of natural oxide [23] and a gold top electrode) on a flexible 50 μm PEN substrate is described. This characterization is relevant for recently reported plastic electronic applications, such as flexible organic transistors using alumina gate insulators [25]. Figure 7 shows a photograph of a thin film capacitor on PEN, demonstrating the flexibility of the fabricated devices. The inset illustrates the layout of the fabricated capacitors. Figure 8 shows leakage current measurements of the capacitor structure. Very small leakage current densities below 1 nA cm$^{-2}$ are obtained up to 1.6 V (corresponding to an electric field strength of 200 MV m$^{-1}$). In the high field region (close to the anodisation potential), tunnelling currents cause leakage through the capacitor. The dielectric properties of such a capacitor are summarized in Fig. 9. For the ≈9 nm thick film, a large capacitance per area of 850 nF cm$^{-1}$ and a loss tangent of $10^{-2}$ at 1 kHz is found. Even at the low-end of the covered frequency ($10^{-4}$ Hz), a loss tangent below 0.1 proves its performance, which corresponds well with the low leakage currents measured in the device. The capacitance per area shows only small

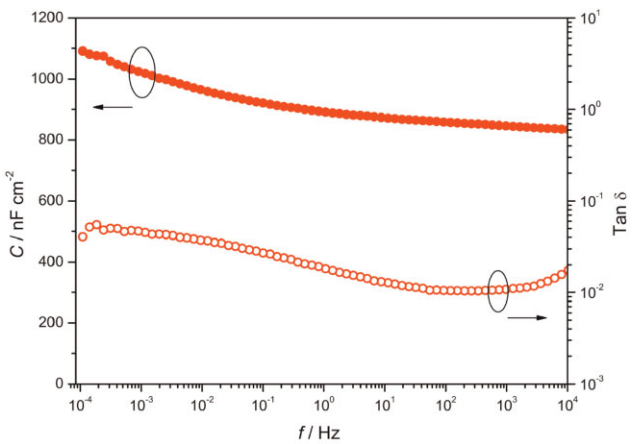


**Figure 9** (online colour at: www.pss-a.com) Capacitance and dielectric losses frequency dependence for a Au/$Al_2O_3$/Al/PEN capacitor.

dispersion over the measured frequency range from $10^4$ to $10^{-4}$ Hz, suggesting the use of such anodized alumina solid state thin film capacitors for plastic electronics.

**4 Conclusions** Ultra-thin anodic oxides grown using the SDC on Al thin films deposited on different plastic substrates were successfully analyzed and compared with oxide films obtained on Al/glass. Slightly bigger anodic formation factors were found for the case of using plastic substrates. This is mainly attributed to an increased wetted area during the anodization due to higher film roughness. However, the oxides formed on plastic substrates have shown very good properties for being used as thin film capacitors. Anodic alumina solid state thin film capacitors on flexible substrates show large, tuneable capacitance per area values with low leakage currents and dielectric losses. Such films may potentially be useful as passive capacitors in flexible electronic circuits.

## References

[1] H. J. Kwon, H. S. Shim, S. Kim, W. Choi, Y. Chun, I. S. Kee, and S. Y. Leeb, Appl. Phys. Lett. **98**, 151904 (2011).
[2] C. J. Brabec, N. S. Sariciftci, and J. C. Hummelen, Adv. Funct. Mater. **11**, 15 (2001).
[3] M. Zirkl, A. Sawatdee, U. Helbig, M. Krause, G. Scheipl, E. Kraker, P. A. Ersman, D. Nilsson, D. Platt, P. Bodö, S. Bauer, G. Domann, and B. Stadlober, Adv. Mater. **23**, 2023 (2011).
[4] D. H. Kim, N. Lu, R. Ma, Y. S. Kim, R. H. Kim, S. Wang, J. Wu, S. M. Won, H. Tao, A. Islam, K. J. Yu, T. Kim, R. Chowdhury, M. Ying, L. Xu, M. Li, H. J. Chung, H. Keum, M. McCormick, P. Liu, Y. W. Zhang, F. G. Omenetto, Y. Huang, T. Coleman, and J. A. Rogers, Science **333**, 838 (2011).
[5] T. Sekitani, U. Zschieschang, H. Klauk, and T. Someya, Nature Mater. **9**, 1015 (2010).
[6] S. F. Tedde, J. Kern, T. Sterzl, J. Fürst, P. Lugli, and O. Hayden, Nano Lett. **9**, 980 (2009).
[7] I. M. Graz, D. P. J. Cotton, and S. P. Lacour, Appl. Phys. Lett. **94**, 071902 (2009).
[8] Y. Y. Hornga, Y. C. Lua, Y. K. Hsuc, C. C. Chena, L.-C. Chenb, and K. H. Chenb, J. Power Sources **195**, 4418 (2010).
[9] W. S. Wong and A. Salleo (eds.), Flexible Electronics: Materials and Applications (Springer, New York, 2009).
[10] A. L. Schulz, Capacitors: Theory, Types and Applications (Nova Science Publ. Inc., New York, 2010).
[11] A. W. Hassel and D. Diesing, J. Electrochem. Soc. **154**, C558 (2007).
[12] A. W. Hassel and D. Diesing, Thin Solid Films **414**, 296 (2002).
[13] J. Virkki, T. Seppälä, L. Frisk, and P. Heino, Microelectron. Reliabil. **50**, 217 (2010).
[14] J. W. Schultze and A. W. Hassel, Encyclopedia of Electrochemistry (Wiley-VCH, Weinheim, 2003), p. 216.
[15] Q. Lua, S. Mato, P. Skeldon, G. E. Thompson, D. Masheder, H. Habazaki, and K. Shimizu, Electrochim. Acta **47**, 2761 (2002).
[16] M. M. Lohrengel, Mater. Sci. Eng. R **11**, 243 (1993).
[17] K. S. Ahn and Y. E. Sung, J. Vac. Sci. Technol. A **19**, 2840 (2001).
[18] A. W. Hassel and D. Diesing, Electrochem. Commun. **4**, 1 (2002).
[19] D. Diesing, A. W. Hassel, and M. M. Lohrengel, Thin Solid Films **342**, 282 (1999).
[20] A. W. Hassel and M. M. Lohrengel, Electrochim. Acta **42**, 3327 (1997).
[21] A. I. Mardare and A. W. Hassel, Rev. Sci. Instrum. **80**, 046106 (2009).
[22] A. W. Hassel, K. Fushimi, and M. Seo, Electrochem. Commun. **1**, 180 (1999).
[23] A. I. Mardare, High Throughput Growth of Anodic Oxides on Valve Metals (VDM Verlag Dr. Müller, Saarbrücken, 2010), p. 17.
[24] A. W. Hassel and M. M. Lohrengel, Mater. Sci. Forum **185**, 581 (1995).
[25] M. Kaltenbrunner, P. Stadler, R. Schwödiauer, A. W. Hassel, N. S. Sariciftci, and S. Bauer, Adv. Mater. **23**, 4892 (2011).

 